

Poynting effect of brain matter in torsion

Valentina Balbi¹, Antonia Trotta², Michel Destrade^{1,2}, and Aisling Ní Annaidh²

¹School of Mathematics, Statistics and Applied Mathematics, NUI Galway, University Road, Galway, Ireland

²School of Mechanical & Materials Engineering, University College Dublin, Belfield, Dublin 4

Abstract

We investigate experimentally and model theoretically the mechanical behaviour of brain matter in torsion. Using a strain-controlled rheometer we perform torsion tests on fresh porcine brain samples. We quantify the torque and the normal force required to twist a cylindrical sample at constant twist rate. Data fitting gives a mean value for the shear modulus $\mu = 900 \pm 312$ Pa and for the second Mooney-Rivlin parameter $c_2 = 297 \pm 189$ Pa, indicative of extreme softness. Our results show that brain always displays a positive Poynting effect; in other words, it expands in the direction perpendicular to the plane of twisting. We validate the experiments with Finite Element simulations and show that when a human head experiences a twisting motion in the horizontal plane, the brain can experience large forces in the axial direction.

1 Introduction

The brain is an extremely soft and fragile tissue, making it hard to test experimentally using the standard protocols in place for soft matter such as elastomers or rubbers [1]. The inflation test is not appropriate for obvious reasons. The uni-axial tensile test requires a dog-bone geometry and clamping, which cannot be realised in practice for brain tissue; instead, the end faces of a cylinder have to be glued to the tension plates, which leads rapidly to an inhomogeneous deformation [2, 3]. The compression test can achieve homogeneous deformation with lubrication of the plates, but only up to about 10% strain, after which it starts to bulge out [4]. By contrast, the simple shear test works well [5, 6] to least 45° tilting angle leading to a maximal stretch of more than 60%. Similarly, as we show in this paper, the torsion test can be implemented readily for brain matter.

Simple shear and torsion tests are particularly useful to study the Poynting effect, a typical nonlinear phenomenon displayed by soft solids. When sheared or twisted those materials tend to elongate (positive Poynting effect [7]) or contract (negative Poynting effect [8]) in the direction perpendicular to the shearing or twisting

plane. This phenomenon has been observed for brain matter in simple shear tests [6]. However, a practical limitation of simple shear tests is that to date there are no shearing devices able to measure and quantify the normal force, which limits the determination of material parameters.

An alternative test is torsion. It can be performed by glueing a cylindrical sample between two parallel plates and then applying a twist to the sample by rotating one plate with respect to the other. In the past, torsion tests on brain matter have been performed using a *rheometer*, at constant strain rates (from 0.05 to 1 s⁻¹) [9] to measure the elastic properties of the tissue and dynamically over a range of frequencies (20-200 Hz) [10] to investigate its viscoelastic behaviour. A comprehensive summary of the results of mechanical tests on brain tissue can be found in two recent reviews [11, 12]. However, in those studies only the torques were recorded. Moreover, torsion was modelled as simple shear, an equivalence which as we show in Section 5, is only valid locally. To the authors' knowledge, the role played by the normal forces arising during torsion has not been investigated yet.

In this work, we perform torsion tests on cylindrical porcine brain samples and measure the torque and the axial force required to twist the samples at a constant twist rate of 300 rad m⁻¹ s⁻¹. In Section 2 we describe the experimental protocols for preparing and testing the brain specimens. In Section 3, we present the collected and filtered data and describe the filtering strategy adopted to keep meaningful experimental measurements. We then accurately model the data with the Mooney-Rivlin model in Section 4 and obtain material parameters of brain matter which compare well with those found from other tests. To further validate the analytical modelling we implement Finite Element (FE) simulations in Abaqus to mimic the experiments and we finally use the estimated mechanical parameters to simulate a rotational head impact.

Our main finding is that brain matter exhibits the normal Poynting effect, i.e. it tends to expand along its axis when twisted [13]. As noted by Rivlin [7], the Poynting effect is a nonlinear elastic effect *par excellence* and cannot be explained by the linearised theory. It was present in all the cylindrical samples we tested, and when we simulated the twisting rapid motion of a head in a Finite Element model, we found that large vertical stresses developed in the whole brain also.

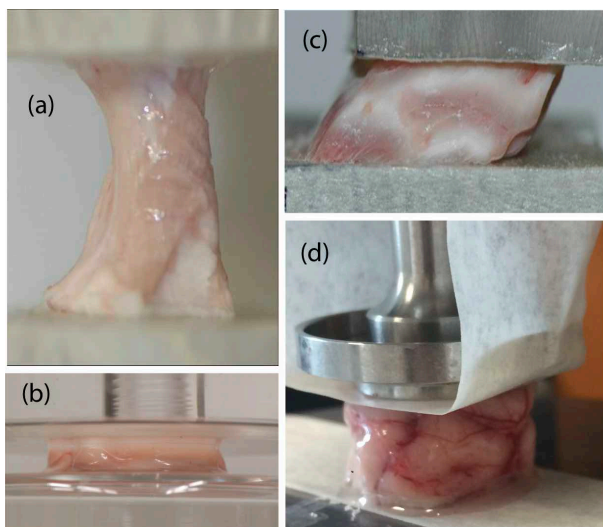


Figure 1: Standard testing protocols for soft solids applied to brain matter (porcine): (a) tensile test with glued ends and (b) compression test with lubricated faces: notice the inhomogeneity of the resulting deformations; (c) simple shear and (d) torsion: here the samples behave as required.

2 Materials and methods

In this section, we give a brief description of the procedure for preparation and testing of the brain samples.

2.1 Tissue preparation

Six fresh porcine heads were obtained from a local abattoir from freshly killed 22 week old mixed sex pigs. The scalp was removed using a scalpel and the cranial bone was removed using an oscillating saw. Following removal of the skull, the meninges tissue was removed using surgical scissors. Finally, following resection of connective and vascular tissue and separation from the spinal cord, the undamaged brain was placed in PBS. The brains had an average (maximum) length, width and height of 7.5 ± 0.3 cm, 6.4 ± 0.3 cm and 3 ± 0.3 cm, respectively. A stainless steel cylindrical punch of 20 mm diameter was used to remove cylinders from each hemisphere as shown in Fig. 2. Each long cylindrical sample was then cut to samples of approximately 10 mm using a scalpel and template. The exact height of the specimen was measured again prior to testing. Mixed grey and white matter cylindrical samples were placed in PBS solution in multi-well plates of 20 mm diameter and placed in a fridge for less than 2 hours while all samples were prepared.

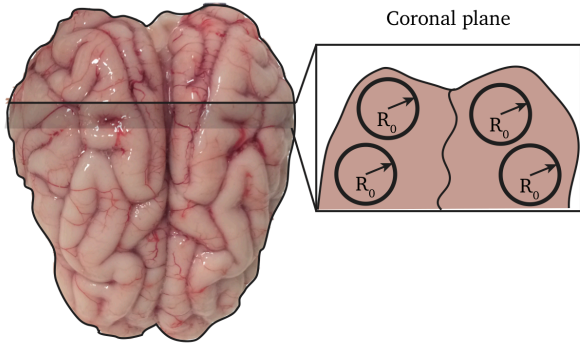


Figure 2: Sketch of the cutting map of a fresh porcine brain (top view). The cylindrical samples were obtained by cutting a slice of brain excised from the coronal plane into cylinders of radius $R_0 = 10$ mm.

2.2 Mechanical Testing

A Discovery HR2 Hybrid Rheometer with parallel plates was used for all mechanical testing. This device has a torque resolution of 0.1 nNm and a normal force resolution of 0.5 mN. To enable easy removal, masking tape was applied to both faces of the parallel plates, and then samples were glued to the tape using cyanoacrylate. All testing was performed at room temperature and the samples were kept hydrated until the beginning of the test. A cylindrical Peltier plate with radius $r_p = 10$ mm was used. The rheometer was controlled through the TRIOS Software (v4.3.1). Each test consisted of a single *stress growth* step for a duration of 10 s. The distance H between the top plate and the bottom of the instrument was adjusted until the normal force was zero at the beginning of each test. The twist rate (angular velocity of the upper plate per unit height) was $\dot{\phi} = 300 \text{ rad m}^{-1} \text{ s}^{-1}$.

3 Experimental Results

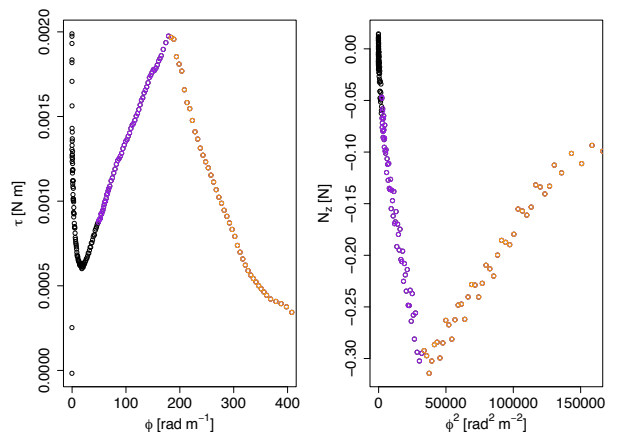
In this section, we describe the filtering procedure required to get a clean set of data, ready for model fitting and parameter estimation.

Figure 3 shows a set of typical output data from the rheometer. In 3(a) the torque τ and the normal force N_z are plotted against the twist ϕ and the twist squared,

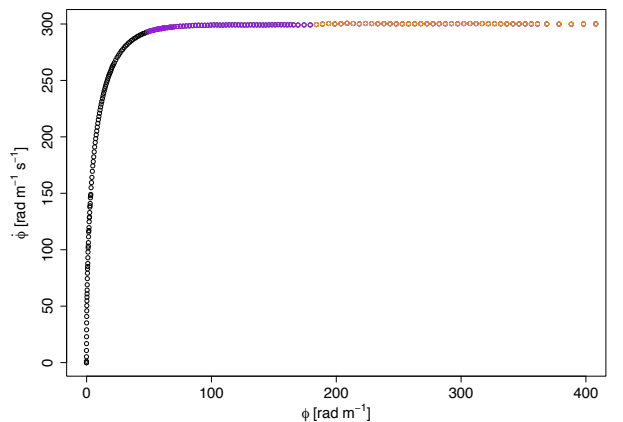
respectively. The output twist ϕ in the plots is the angle of rotation α per unit length $\phi = \alpha/H$. From the data shown in Figure 3(a), we identify three regions, for both the torque and the force data: (i) a noisy region (in black), at the very beginning of the test; (ii) a linear region (in purple) bounded by a maximum (minimum), and (iii) a decaying region (in orange) towards the end of the experiment.

The initial noisy region is due to the delay time of the instrument in reaching a constant twist rate. The plot in Figure 3(b) shows the twist rate against the twist and clearly highlights the initial region where the upper plate is accelerating to reach the constant twist rate $\dot{\phi} = 300 \text{ rad m}^{-1} \text{ s}^{-1}$. The plots in Figure 3 (c) further show that some data were actually generated at twist rate lower than $300 \text{ rad m}^{-1} \text{ s}^{-1}$. Only the data generated at $300 \text{ rad m}^{-1} \text{ s}^{-1}$ was thus considered in the following analysis.

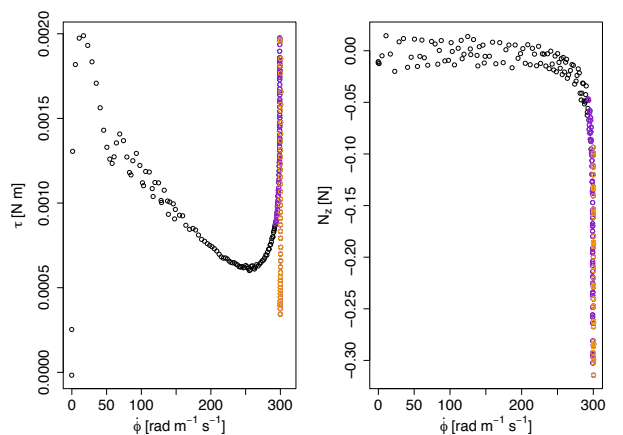
The other filtering criterion is the breaking point of the sample, which is identified clearly by a steep drop



(a) Representative torque and normal force output



(b) Strain rate monitoring



(c) Data output vs strain rate

Figure 3: Original collected data: (a, left) torque against twist and (a, right) normal force against twist squared; (b) twist rate against twist; (c, left) torque and (c, right) normal force against twist rate. Black data: ramping towards the constant twist rate, see (b); Purple: proper data of torsion; Orange: data after breaking point, see (a).

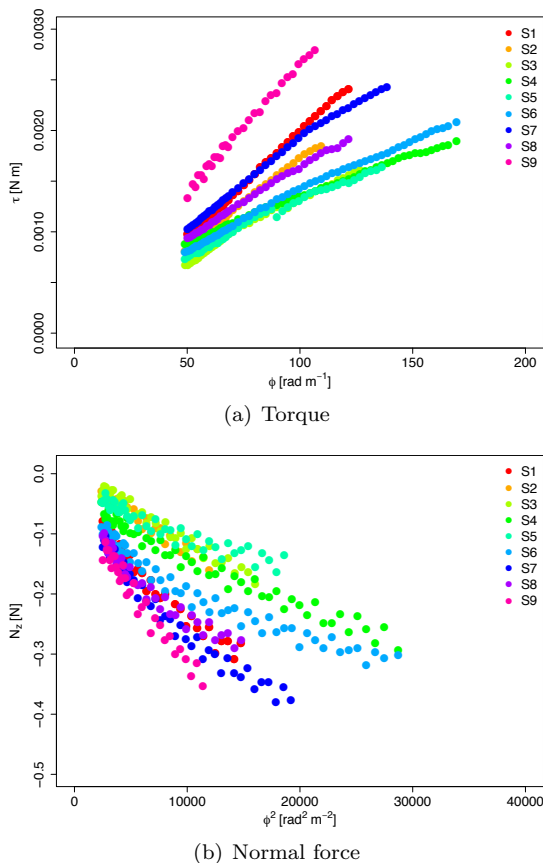


Figure 4: Results of the torsion tests performed at a twist rate $\dot{\phi} = 300 \text{ rad m}^{-1} \text{ s}^{-1}$ on nine cylindrical samples of brain tissue excised from the coronal plane. (a) Torque τ vs twist ϕ and (b) normal force N_z vs twist squared ϕ^2 , measured for cylindrical samples with initial radius $R_0 = 10 \text{ mm}$.

and rise in the plots of Figure 3 (a), indicating that an irreversible change in the mechanical response of the tissue occurred. Therefore, all data points after the breaking point were discarded.

The remaining “good” data obtained from nine samples S_1, \dots, S_9 are shown in Figure 4.

4 Modelling

To fit the experimental data and get a quantitative estimation of the behaviour of the brain in torsion, we first analyse the data, and then reproduce the mechanical tests theoretically. Finally we perform Finite Element simulations in Abaqus.

4.1 Theory

Here we calculate the torque τ and the normal force N_z required to maintain a cylindrical sample of initial radius R_0 and initial height L_0 in a state of torsion.

As mentioned in Section 2.2, the normal force was set to zero before commencing each test. However, the force transducer of the HR2 rheometer has a sensitivity of 0.01 N, so that variations of the force within that range are not detected by the instrument. We therefore expect that the sample undergoes a small contraction prior to the transducer picking up a meaningful value for the force. Mathematically, we superpose an axial contraction to the actual rotation so that the total deformation is written in cylindrical coordinates as follows:

$$r = R/\sqrt{\lambda}, \quad \theta = \Theta + \phi\lambda Z, \quad z = \lambda Z, \quad (1)$$

where λ is the (tensile or compressive) pre-stretch, $\phi = \alpha/(\lambda L_0)$ is the twist per unit height and α is the angle of rotation in radians. The corresponding deformation

gradient \mathbf{F} is then:

$$\mathbf{F} = \begin{pmatrix} 1/\sqrt{\lambda} & 0 & 0 \\ 0 & 1/\sqrt{\lambda} & r\phi\lambda \\ 0 & 0 & \lambda \end{pmatrix}. \quad (2)$$

We are interested in the elastic behaviour of brain matter, which we assume to be isotropic and incompressible. In view of the linear dependence of the torque with respect to the twist highlighted by the results in Figure 4, we conclude that the constitutive behaviour of the brain must be modelled with a Mooney-Rivlin strain energy function [14]:

$$W = c_1(I_1 - 3) + c_2(I_2 - 3), \quad (3)$$

where c_1, c_2 are constants, $I_1 = \text{tr}[\mathbf{B}]$, $I_2 = \text{tr}[\mathbf{B}^{-1}]$ and $\mathbf{B} = \mathbf{F}\mathbf{F}^T$. For this model the shear modulus is $\mu = 2(c_1 + c_2)$. The corresponding constitutive equation for the Cauchy stress $\boldsymbol{\sigma}$ reads:

$$\boldsymbol{\sigma} = 2c_1\mathbf{B} - 2c_2\mathbf{B}^{-1} - p\mathbf{I}, \quad (4)$$

where p is the Lagrange multiplier introduced to enforce incompressibility and \mathbf{I} is the identity matrix.

The principal stretches are the square roots of the eigenvalues of \mathbf{B} . The intermediate stretch $\lambda_1 = 1$ is associated with the radial direction, and the maximum and minimum stretches λ_2 and λ_3 are obtained by solving the following equations:

$$(\lambda_2\lambda_3)^2 = \frac{1}{\lambda}, \quad \lambda_2^2 + \lambda_3^2 = \frac{1}{\lambda} + \lambda^2 + (\lambda\phi r)^2. \quad (5)$$

The elastic equilibrium of the deformation is translated as the following problem:

$$\frac{d}{dr}\sigma_{rr}(r) + \frac{\sigma_{rr}(r) - \sigma_{\theta\theta}(r)}{r} = 0, \quad \sigma_{rr}(r_0) = 0, \quad (6)$$

with solution:

$$\begin{aligned} \sigma_{rr}(r) &= c_1(r^2 - r_0^2)\lambda^2\phi^2, \\ \sigma_{\theta\theta}(r) &= c_1(3r^2 - r_0^2)\lambda^2\phi^2, \\ \sigma_{zz}(r) &= c_1\left(2\frac{\lambda^3 - 1}{\lambda} + (r^2 - r_0^2)\lambda^2\phi^2\right) \\ &\quad + 2c_2\left(\frac{\lambda^3 - 1}{\lambda^2} + r^2\lambda\phi^2\right), \\ \sigma_{\theta z}(r) &= 2(c_2 + c_1\lambda)r\lambda\phi. \end{aligned} \quad (7)$$

These formulas were first established by Rivlin [7], see Appendix A for details.

Now, the torque $\tau = 2\pi \int_0^{R_0/\sqrt{\lambda}} r^2 \sigma_{\theta z}(r) dr$ and the normal force $N_z = 2\pi \int_0^{R_0/\sqrt{\lambda}} r \sigma_{zz}(r) dr$ that have to be applied to the cylinder to maintain the deformation in (1) are:

$$\tau = \pi R_0^4 \left(c_1 + \frac{c_2}{\lambda}\right) \phi = \mathcal{A} \phi \quad (8)$$

$$\begin{aligned} N_z &= -2\pi R_0^2 \left(c_1 + \frac{c_2}{\lambda}\right) \left(\frac{1 - \lambda^3}{\lambda^2}\right) - \pi R_0^4 \left(\frac{c_1}{2} + \frac{c_2}{\lambda}\right) \phi^2 \\ &= \mathcal{C} + \mathcal{B} \phi^2 \end{aligned} \quad (9)$$

where the constants $\mathcal{A}, \mathcal{B}, \mathcal{C}$ introduced above and the parameters c_1, c_2 are linked by the following relations:

$$c_1 = 2 \frac{\mathcal{A} + \mathcal{B}}{\pi R_0^4}, \quad \frac{c_2}{\lambda} = -\frac{\mathcal{A} + 2\mathcal{B}}{\pi R_0^4}, \quad (10)$$

and the pre-stretch λ is the unique real and positive root of the following cubic:

$$2\mathcal{A}(\lambda^3 - 1) - \mathcal{C}R_0^2\lambda^2 = 0. \quad (11)$$

Note, as expected for the Mooney-Rivlin model, the linear dependence of the torque on the twist and of the

normal force on the twist squared, see (8) and (9). The coefficient \mathcal{B} is associated with the Poynting effect displayed by the sample and is due almost entirely to the twist, whereas the coefficient \mathcal{C} accounts for the pre-stretch only. When $\lambda = 1$, i.e. in *pure torsion*, we have $\mathcal{A} = \pi R_0^4(c_1 + c_2)$, $\mathcal{B} = -\pi R_0^4(c_1/2 + c_2)$, $\mathcal{C} = 0$. The values of λ in Table 2 show that samples S_2 and S_3 experience less than 1% pre-stretch; hence for those two samples, \mathcal{B} provides an effective measure of the exact Poynting effect, i.e. in the absence of a normal compressive force, the samples would expand axially.

4.2 Parameters estimation

To fit the data in Figure 4, we use the open-source software RStudio (version 1.1.383). The function `lm` (from the package *stats*) allows to perform a linear regression on the data sets $\{\phi, \tau\}$ and $\{\phi^2, N_z\}$. By calling the function `lm` on the set $\{\phi, \tau\}$ we obtain the coefficient \mathcal{A} from equation (8) and the linear regression on $\{\phi^2, N_z\}$ gives us the coefficients \mathcal{B}, \mathcal{C} appearing in equation (9).

Moreover, the fit on $\{\phi^2, N_z\}$ uses a weighted (with respect to ϕ^2) least squares method. Finally, we input the coefficients \mathcal{A}, \mathcal{B} and \mathcal{C} into equations (10) to get the elastic parameters c_1 and c_2 . The results of the linear regression are shown in Table 1. The mean values for the elastic parameters are $\mu = 900$ Pa and $c_2 = 297$ Pa, respectively. The dimensions of the nine samples after the compression are summarised in Table 2, where the length l_0 and radius r_0 are given for each sample, as well as the pre-stretch computed from (11) and the maximum values of the highest principal stretch λ_2^{\max} , attained at breaking point on the periphery of the top face.

sample	μ [Pa]	c_2 [Pa]	R_τ^2	$R_{N_z}^2$
S_1	1232.50	294.45	0.999	0.946
S_2	1092.31	235.84	0.998	0.939
S_3	766.95	310.60	0.988	0.966
S_4	491.14	201.22	0.996	0.958
S_5	656.96	59.68	0.988	0.87
S_6	644.59	113.75	0.994	0.92
S_7	952.36	347.26	0.993	0.947
S_8	803.12	401.41	0.997	0.925
S_9	1460.17	710.29	0.995	0.962
mean \pm SD	900 \pm 312	297 \pm 189		

Table 1: Estimated elastic parameters: the shear modulus $\mu = 2(c_1 + c_2)$, the Mooney-Rivlin parameter c_2 and the coefficient of determination R^2 . Mean values with standard deviation for μ and c_2 are also calculated in the last row.

sample	λ	l_0 [mm]	r_0 [mm]	λ_2^{\max}
S_1	0.93	12.62	10.36	1.82
S_2	0.99	16.02	10.05	1.73
S_3	0.99	15.92	10.05	1.81
S_4	0.89	12.95	10.59	2.14
S_5	0.94	13.26	10.31	1.85
S_6	0.85	14.19	10.84	2.04
S_7	0.89	9.51	10.59	1.87
S_8	0.89	12.22	10.59	1.68
S_9	0.95	10.14	10.26	1.69

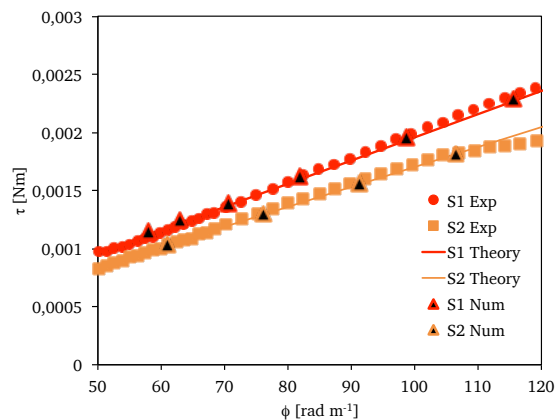
Table 2: Geometry of the samples after pre-compression, prior to twisting: the estimated axial stretch λ , the length $l_0 = \lambda L_0$ (measured by the instrument), the radius $r_0 = 1/\sqrt{\lambda} R_0$ of the nine samples and the maximum value of the greatest principal stretch λ_2 before sample breaking.

4.3 Computational validation

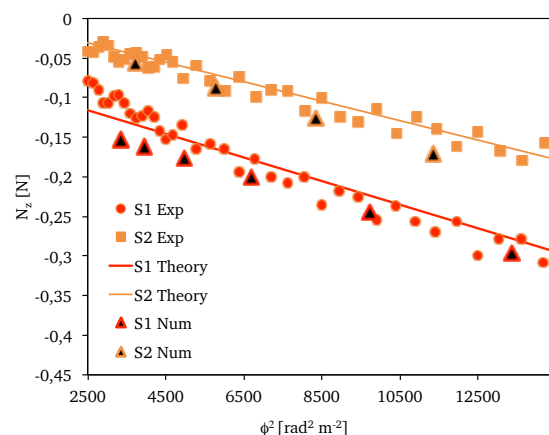
We performed brain torsion simulations using ABAQUS Standard 6.14-1 to validate our analytical modelling of the deformation. The initial cylindrical geometry of the sample was obtained by setting the radius $R_0 = 10$ mm and the height $L_0 = l_0/\lambda$, calculated according to Table 2. We used a mesh of 78,750 hexahedral elements (C3D8) with hybrid formulation to reproduce exact incompressibility and we assigned a Mooney Rivlin model with material parameters in Table 1 to account for hyperelasticity.

To simulate the twist, we first defined a reference point at the centre of the top surface of the cylinder, which we then coupled with all points on the surface, and finally we assigned a rotational displacement around the longitudinal axis (ramp form of amplitude 3 rad) whilst setting the other degrees of freedom to zero. The bottom surface of the cylinder was encastred. The output variables were the resultant axial force (RF3) and torque (RM3).

To perform the simulations we chose two specimens: S_1 and S_2 . An additional step, prior to the torsion, was added to simulate the 7% pre-compression (see Table 2) undergone by S_1 . The results are shown in Fig. 5. We see that the numerical simulations validate the predictions of the analytical model described in Section 4.1. The torque and the normal force calculated in Abaqus are consistent with the analytical predictions and the measured data for both cases with and without pre-compression (S_1 and S_2 , respectively). We note that there is a small mismatch between the analytical and the numerical normal force for S_1 . This is due to the longitudinal bulging of the sample occurring during the 7%



(a) Torque



(b) Normal force

Figure 5: Comparison of the resultant torque τ and normal force N_z for S_1 and S_2 . Results of the numerical simulations in Abaqus (triangles), analytical predictions with the models (8) and (9) (solid lines) and experimental data (red circles for S_1 and orange squares for S_2).

compression phase, which results in a non-homogeneous deformation along the axis of the cylinder.

5 Discussion and conclusions

Now we compare the results obtained here for torsion tests with those obtained elsewhere for simple shear tests and for torsion modelled as simple shear.

We begin by recalling that the deformation gradient for uni-axial compression in the Z direction, followed by simple shear of amount κ in the YZ plane, has the form [15]

$$\mathbf{F} = \begin{pmatrix} 1/\sqrt{\lambda} & 0 & 0 \\ 0 & 1/\sqrt{\lambda} & \lambda\kappa \\ 0 & 0 & \lambda \end{pmatrix}. \quad (12)$$

Hence, we see from comparison with (2) that there is a formal connection between torsion and simple shear. However, the equivalence is *local* only, as simple shear is homogeneous but torsion is not: the amount of “shear” experienced by an element in torsion ($\kappa = r\phi = r\alpha/H$) depends on the dimensions of the sample and the position of the element. Thus, it does not make sense to compare the amount of shear and the shear rate experienced by all elements in a simple shear experiment with the amount of “shear” and the “shear” rate experienced by a given element at a given location for a given sample dimension in a torsion experiment. Despite this disconnect, finite shear and torsion are often confused in the literature, and torsion experiments in rheometers are routinely modelled as simple shear, see for example the papers cited in the extensive review by Chatelin et al. [11].

Here we note that the results presented in Table 1 show that cylindrical samples of brain matter with initial radius $R_0 = 10$ mm twisted at a twist rate $\dot{\phi} = 300 \text{ rad m}^{-1}\text{s}^{-1}$ behave as Mooney-Rivlin materials with a shear modulus $\mu = 900 \pm 312 \text{ Pa}$. This value is in the same range of values found by Rashid et al. [16] when a block of porcine brain matter was sheared at a shear rate of $\dot{\kappa} = 30 \text{ s}^{-1}$, estimated to be conducive to diffuse axonal injury [17, 18]. Moreover, from Table 2 we note that the values of the principal stretch (greatest stretch) λ_2 at the breaking point are in the range $1.67 - 2.14$ which corresponds to extensions of 67% to 114%. These values of strain are well above the estimate axonal strain thresholds associated to diffuse axonal injury (> 0.05) [19] and to white matter damage in the optical nerve (> 0.34) [20].

In addition, here we are able to directly estimate the second Mooney-Rivlin coefficient c_2 from the normal force data and thus provide a direct measure of the Poynting effect. This quantity cannot be measured from shear stress data alone, although its sign (positive for porcine brain matter) can be deduced by piercing a hole in one of the plattens [6]. We note also that in contrast to simple shear, where a neo-Hookean material ($c_2 = 0$) does not display the Poynting effect [6], the same material does have a non-zero normal force in torsion [21].

Our conclusion is that brain matter exhibits a real and large Poynting effect in torsion, which is bound to lead to the development of large normal forces in an impacted brain.

In order to investigate the existence and magnitude of axial forces during twisting head impacts, we used Abaqus/Explicit to simulate a rotational impact with the University College Dublin Brain Trauma Model (UCDBTM) developed by Horgan and Gilchrist [22].

We applied a rotational acceleration in the axial plane to the centre of gravity of the head, peaking at 2.170 rad s^{-2} . This value of rotational acceleration is in the range of accelerations experienced in boxing [23]. We used the mean values of the estimated parameters μ

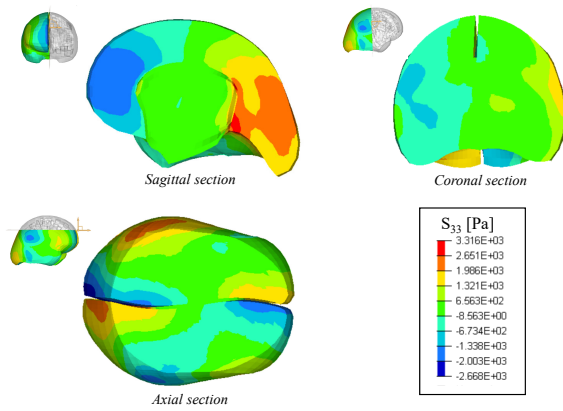


Figure 6: Results of the FE simulations of a rotational head impact, performed with the UCDBT Model. Distribution of the stress component S_{33} across the *Sagittal*, *Coronal* and *Axial* planes.

and c_2 in Table 1 to model the mechanical behaviour of the brain matter. In Fig 6, the distribution of the axial stress component S_{33} (where \mathbf{S} is the deviatoric part of the Cauchy stress) throughout the brain is shown for a rotational angle of $\alpha = 0.52 \text{ rad}$. The three sections in the sagittal, coronal and axial planes, respectively, highlight areas where the stress reaches peaks of magnitude in the thousands of Pa. Therefore the high normal stresses developing during rotational impacts could potentially contribute to Traumatic Brain Injury (TBI) during this type of impact. The results presented in this work thus open the path towards further studies to quantify the role played by normal forces in TBI, in particular with a view to define more accurate threshold criteria for TBI.

Appendix A

By integrating the first of (6) together with the initial condition we obtain:

$$\begin{aligned} \sigma_{rr}(r) &= \int_r^{r_0} \frac{\Sigma_r - \Sigma_\theta(r)}{r} dr \\ \sigma_{\theta\theta}(r) &= \Sigma_\theta(r) - \Sigma_r + \int_r^{r_0} \frac{\Sigma_r - \Sigma_\theta(r)}{r} dr \\ \sigma_{zz}(r) &= \Sigma_z(r) - \Sigma_r + \int_r^{r_0} \frac{\Sigma_r - \Sigma_\theta(r)}{r} dr \\ \sigma_{\theta z}(r) &= c_1 B_{\theta z}(r) - c_2 \frac{B_{\theta z}(r)}{\Sigma} \end{aligned} \quad (13)$$

where

$$\begin{aligned} \Sigma_r - \Sigma_\theta(r) &= 2c_1 (B_{rr} - B_{\theta\theta}(r)) + 2c_2 \left(\frac{B_{zz}}{\Sigma} - \frac{1}{B_{rr}} \right) \\ \Sigma_z(r) - \Sigma_r &= 2c_1 (B_{zz} - B_{rr}) + 2c_2 \left(\frac{1}{B_{rr}} - \frac{B_{\theta\theta}(r)}{\Sigma} \right) \\ \text{and } \Sigma &= B_{zz} B_{\theta\theta}(r) - B_{\theta z}^2(r) = 1/B_{rr} \end{aligned} \quad (14)$$

Then, by substituting (2) into (14) and then into (13) we obtain (7).

Conflicts of interest

There are no conflicts to declare.

Acknowledgements

We thank Badar Rashid for Figures 1(a), (b), (c); David McManus for help with the dissection of pig heads; Xiaolin Li for technical assistance with the rheometer; Christiane G6rgen for help with fitting in

RStudio and Giuseppe Saccomandi for insightful discussions on the modelling of torsion. The work has received funding from the European Union’s Horizon 2020 Research and Innovation Programme under the Marie Skłodowska-Curie grant agreement No.705532 (Valentina Balbi and Michel Destrade).

References

- [1] British Standards. Physical Testing of Rubber. General. British Standards Institution. 2012;BS 903-0:2012.
- [2] Miller K, Chinzei K. Mechanical properties of brain tissue in tension. *Journal of Biomechanics*. 2002;35(4):483–490.
- [3] Rashid B, Destrade M, Gilchrist MD. Inhomogeneous deformation of brain tissue during tension tests. *Computational Materials Science*. 2012;64:295–300.
- [4] Rashid B, Destrade M, Gilchrist MD. Mechanical characterization of brain tissue in compression at dynamic strain rates. *Journal of the Mechanical Behavior of Biomedical Materials*. 2012;10:23–38.
- [5] Donnelly B, Medige J. Shear properties of human brain tissue. *Journal of Biomechanical Engineering*. 1997;119(4):423–432.
- [6] Destrade M, Gilchrist M, Murphy JG, Rashid B, Saccomandi G. Extreme softness of brain matter in simple shear. *International Journal of Non-Linear Mechanics*. 2015;75:54–58.
- [7] Rivlin RS. Large elastic deformations of isotropic materials VI. Further results in the theory of torsion, shear and flexure. *Philosophical Transactions of the Royal Society of London A*. 1949;242(845):173–195.
- [8] Janmey PA, McCormick ME, Rammensee S, Leight JL, Georges PC, MacKintosh FC. Negative normal stress in semiflexible biopolymer gels. *Nature materials*. 2007;6(1):48.
- [9] Bilston LE, Liu Z, Phan-Thien N. Large strain behaviour of brain tissue in shear: some experimental data and differential constitutive model. *Biorheology*. 2001;38(4):335–345.
- [10] Arbogast KB, Margulies SS. Material characterization of the brainstem from oscillatory shear tests. *Journal of biomechanics*. 1998;31(9):801–807.
- [11] Chatelin S, Constantinesco A, Willinger R. Fifty years of brain tissue mechanical testing: From in vitro to in vivo investigations. *Biorheology*. 2010;47(5-6):255–276.
- [12] Goriely A, Geers MG, Holzapfel GA, Jayamohan J, Jérusalem A, Sivaloganathan S, et al. Mechanics of the brain: perspectives, challenges, and opportunities. *Biomechanics and modeling in mechanobiology*. 2015;14(5):931–965.
- [13] Poynting JH. On pressure perpendicular to the shear planes in finite pure shears, and on the lengthening of loaded wires when twisted. *Proceedings of the Royal Society of London A*. 1909;82(557):546–559.
- [14] Mangan R, Destrade M, Saccomandi G. Strain energy function for isotropic non-linear elastic incompressible solids with linear finite strain response in shear and torsion. *Extreme Mechanics Letters*. 2016;9:204–206.
- [15] Rajagopal K, Wineman AS. New universal relations for nonlinear isotropic elastic materials. *Journal of Elasticity*. 1987;17(1):75–83.
- [16] Rashid B, Destrade M, Gilchrist MD. Mechanical characterization of brain tissue in simple shear at dynamic strain rates. *Journal of the Mechanical Behavior of Biomedical Materials*. 2013;28:71–85.
- [17] Morrison B, Cater HL, Wang CC, Thomas FC, Hung CT, Ateshian GA, et al. A tissue level tolerance criterion for living brain developed with an in vitro model of traumatic mechanical loading. *SAE Technical Paper*; 2003.
- [18] Morrison III B, Cater HL, Benham CD, Sundstrom LE. An in vitro model of traumatic brain injury utilising two-dimensional stretch of organotypic hippocampal slice cultures. *Journal of neuroscience methods*. 2006;150(2):192–201.
- [19] Yap YC, King AE, Guijt RM, Jiang T, Blizzard CA, Breadmore MC, et al. Mild and repetitive very mild axonal stretch injury triggers cytoskeletal mislocalization and growth cone collapse. *PloS one*. 2017;12(5):e0176997.
- [20] Bain AC, Meaney DF. Tissue-level thresholds for axonal damage in an experimental model of central nervous system white matter injury. *Journal of biomechanical engineering*. 2000;122(6):615–622.
- [21] Horgan CO, Murphy JG. Reverse Poynting effects in the torsion of soft biomaterials. *Journal of Elasticity*. 2015;118(2):127–140.
- [22] Horgan TJ, Gilchrist MD. The creation of three-dimensional finite element models for simulating head impact biomechanics. *International Journal of Crashworthiness*. 2003;8(4):353–366.
- [23] Walilko T, Viano DC, Bir CA. Biomechanics of the head for Olympic boxer punches to the face. *British Journal of Sports Medicine*. 2005;39(10):710–719.